DRAFT: Probing for high momentum protons in ^4He via the $^4He(e,e'p)^3H$ reaction

S. Iqbal,[1] F. Benmokhtar,[2] M. Ivanov,[3] N. See,[1] D. Finton,[2] K. Aniol,[1,*] D. W. Higinbotham,[4] S. Gilad,[5] A. Saha, [4,†] P. Solvignon,[4,†] Z. Ye,[6] V. Sulkosky,[5,20] P. Aguilera,[7] Z. Ahmed,[8] H. Albataineh,[8] K. Allada,[10] B. Anderson,[11] D. Anez,[12] J. Annand,[13] W. Armstrong,[14] J. Arrington,[15] T. Averett,[16] T. Badman,[17] H. Baghdasaryan,[6] X. Bai,[18] A. Beck,[19] S. Beck,[19] V. Bellini,[20] W. Bertozzi,[5] J. Bittner,[21] W. Boeglin,[22] A. Camsonne,[4] C. Chen,[23] J.-P. Chen,[4] K. Chirapatpimol,[6] E. Cisbani,[24] M. M. Dalton,[4] A. Daniel,[26] D. Day,[6] C. W. de Jager,[4,6] R. De Leo,25 W. Deconinck,[15] M. Defurne,[27] D. Flay,[13] N. Fomin,[28] S. Frullani,[25] E. Fuchey,[13] F. Garibaldi,[25] D. Gaskell,[4] R. Gilman,[28,4] O. Glamazdin,[29] C. Gu,[30] P. Gueye,[31] D. Hamilton,[12] C. Hanretty,[32] J.-O. Hansen,[4] M. Hashemi Shabestari,[6] O. Hen,[33] T. Holmstrom,[20] M. Huang,[32] G. Jin,[6] N. Kalantarians,[34] H. Kang,[35] A. Kelleher,[5] M. Khandaker,[4] I. Korover,[33] J. LeRose,[4] J. Leckey,[36] R. Lindgren,[17] E. Long,[16] J. Mammei,[37] N. Muangma,[5] D. J. Margaziotis,[1] P. Markowitz,[22] A. Marti Jimenez-Arguello,[38] D. Meekins,[4] Z. Meziani,[13] R. Michaels,[4] M. Mihovilovic,[39] P. Monaghan,[5,23] C. Munoz Camacho,[38] B. Norum,[5,40] K. Pan,[5] E. Piasetzky,[33] S. Phillips,[16] I. Pomerantz,[33,41] M. Posik,[13] V. Punjabi,[42] X. Qian,[34] Y. Qiang,[34] X. Qiu,[34] A. Rakhman,[6] P. E. Reimer,[14] S. Riordan,[5,45] G. Ron,[46] O. Rondon-Aramayo,[4] E. Schulte,[30] L. Selvy,[10] A. Shahinyan,[47] R. Shneor,[34] S. Sirca,[48] J. Sjoegren,[13] K. Slifer,[17] N. Sparveris,14 R. Subedi,[6] W. Tireman,[50] J.M.Udias,[51] D. Wang,[6] J. W. Watson,[11] L. B. Weinstein,[9] B. Wojtsekhowski,[4] S. A. Wood,[4] W. Yan,[50] I. Yaron,[33] X. Zhan,[6] J. Zhang,[4] Y. Zhang,[30] B. Zhao,[16] Z. Zhao,[6] X. Zheng,[6] P. Zhu,[50] R. Zielinski,[17] and (The Jefferson Lab Hall A Collaboration)[1,*]

[1] *California State University, Los Angeles, Los Angeles, California 90032, USA*
[2] *Duquesne University, Pittsburgh, Pennsylvania 15282, USA*
[3] *Bulgarian Academy of Sciences, Bulgaria,*
[4] *Thomas Jefferson National Accelerator Facility, Newport News, Virginia 23606, USA*
[5] *Massachusetts Institute of Technology, Cambridge, Massachusetts 02139, USA*
[6] *University of Virginia, Charlottesville, Virginia 22904, USA*
[7] *Syracuse University, Syracuse, New York 13244, USA*
[8] *Institut de Physique Nucleaire (UMR 8608), CNRS/IN2P3Universite Paris-Sud, F-91406 Orsay Cedex, France*
[9] *Old Dominion University, Norfolk, Virginia 23529, USA*
[10] *University of Kentucky, Lexington, Kentucky 40506, USA*
[11] *Kent State University, Kent, Ohio 44242, USA*
[12] *Saint Marys University, Halifax, Nova Scotia, Canada*
[13] *University of Glasgow, Glasgow G12 8QQ, Scotland, United Kingdom*
[14] *Temple University, Philadelphia, Pennsylvania 19122, USA*
[15] *Physics Division, Argonne National Laboratory, Argonne, Illinois 60439, USA*
[16] *College of William and Mary, Williamsburg, Virginia 23187, USA*
[17] *University of New Hampshire, Durham, New Hampshire 03824, USA*
[18] *China Institute of Atomic Energy, Beijing, China*
[19] *Nuclear Research Center Negev, Beer-Sheva, Israel*
[20] *Universita di Catania, Catania, Italy*
[21] *Longwood University, Farmville, Virginia 23909, USA*
[22] *Florida International University, Miami, Florida 33199, USA*
[23] *Hampton University, Hampton, Virginia 23668, USA*
[24] *INFN, Sezione Sanita and Istituto Superiore di Sanita, 00161 Rome, Italy*
[25] *Ohio University, Athens, Ohio 45701, USA*
[26] *INFN, Sezione di Bari and University of Bari, I-70126 Bari, Italy*
[27] *CEA Saclay, F-91191 Gif-sur-Yvette, France*
[28] *University of Tennessee, Knoxville, Tennessee 37996, USA*
[29] *Rutgers, The State University of New Jersey, Piscataway, New Jersey 08855, USA*
[30] *Kharkov Institute of Physics and Technology, Kharkov 61108, Ukraine*
[31] *Los Alamos National Laboratory, Los Alamos, New Mexico 87545, USA*
[32] *Florida State University, Tallahassee, Florida 32306, USA*
[33] *Duke University, Durham, North Carolina 27708, USA*
[34] *Tel Aviv University, Tel Aviv 69978, Israel*
[35] *University of Texas, Houston, Texas 77030, USA*
[36] *Seoul National University, Seoul, Korea,*
[37] *Indiana University, Bloomington, Indiana 47405, USA*
[38] *Virginia Polytechnic Institute and State University, Blacksburg, Virginia 24061, USA*
[39] *Universite Blaise Pascal/IN2P3, F-63177 Aubiere, France*
[40] *Jozef Stefan Institute, Ljubljana, Slovenia*
[41] *Mississippi State University, Mississippi State, Mississippi 39762, USA*

[42] The University of Texas at Austin, Austin, Texas 78712, USA
[43] Norfolk State University, Norfolk, Virginia 23504, USA
[44] Lanzhou University, Lanzhou, China
[45] University of Massachusetts, Amherst, Massachusetts 01006, USA
[46] Racah Institute of Physics, Hebrew University of Jerusalem, Jerusalem, Israel
[47] Yerevan Physics Institute, Yerevan 375036, Armenia
[48] University of Ljubljana, Ljubljana, Slovenia
[49] Northern Michigan University, Marquette, Michigan 49855, USA
[50] University of Science and Technology, Hefei, China
[51] Complutense University de Madrid, Spain

Experimental cross sections for the 3-body breakup $^4He(e,e'p)X$ up to $P_{miss} = 0.632GeV/c$ at $x_B = 1.24$ and $Q^2 = 2(GeV/c)^2$ are reported. The data are compared to Relativistic Distorted Wave Impulse Approximation(RDWIA) calculations for $^4He(e,e'p)^3H$ reactions. Significantly more events in the triton mass region are measured for $P_{miss} > 0.45GeV/c$ than are predicted by the theoretical model.

I. INTRODUCTION

Nucleon momentum distributions in atomic nuclei are known to be governed by an average nuclear potential plus additional nucleon-nucleon multi body interactions. Momentum distributions below the Fermi momentum essentially reflect the size of the "box" in which the nucleons are contained. One way to model this distribution is in the simplest limit of a cluster model where a given nucleon interacts with the average potential of the other nucleons. For momenta greater than the Fermi momentum the cluster models of nuclear structure provide enhanced strength in the momentum distribution by allowing nucleon-nucleon spatial distributions to become shorter than the average nucleon-nucleon spacing. Experimental access to proton momentum disributions is possible through the missing momentum observable, p_m, in the $A(e,e'p)X$ reaction, $\vec{p}_X = \vec{p}e - \vec{p}_{e'} - \vec{p}p$, $p_m = |\vec{p}_X|$. Interpretation of cross sections $\sigma(p_m)$ to deduce nucleon momentum distributions requires the inclusion of final state interactions in the outgoing $(e'pX)$ system.

Microscopic nuclear structure calculations based on realistic two and three body nucleon-nucleon calculations are available for low mass nuclei [1]. In the case of ^4He proton momentum distributions have been calculated for proton-triton(pt) and deuteron-deuteron(dd) clusters. Recent measurements of proton-nucleon coincidences in the $^4He(e,e'pN)$ reaction [2] have shown strong correlations of back to back emission of nucleon pairs for large missing momentum $p_m > 400\ MeV/c$. Moreover, the increasing pair ratio $\frac{\#pp}{\#pn}$ as a function of $p_m > 400\ MeV/c$ is interpreted as a sign that the nucleon-nucleon interaction switches from the tensor interaction to the strong repulsive short range interaction. Besides nucleon-nucleon correlations the experiment also obtained data on the pt final hadronic state.

This paper provides experimental differential cross sections, $\frac{d\sigma^5}{d\Omega_p d\Omega_e dE_e}$, over a range of missing momenta, $25 < p_m < 632\ MeV/c$, based on the $^4He(e,e'p)3N$ reaction under the same kinematic conditions as the short range correlation experiment [2], where 3N = ^3H and X.

II. EXPERIMENTAL METHOD

A. Spectrometer settings

Experiments E07006 [2] and E08009 [3] at the Jefferson National Accelerator Facility ran in February, March and April of 2011. Data for kinematic settings of 0.153 and 0.353 GeV/c missing momentum were obtained using electron beam currents between $47\mu A$ to $60\mu A$, for E08009. The details for E08009 are described in a thesis [3], [4]. In addition to these kinematic settings the Short Rangle Correlation(SRC) [2] experiment also obtained data at kinematic settings out to 0.632 GeV/c missing momentum including the two body break up channel p + triton. These higher missing momenta data were collected using about 4 to 5 μA electron beam currents but sufficient accumulated charge was measured to be able to extract cross sections beyond the original goal set for E08009. Moreover, the large acceptances of the Hall A spectrometers allowed for cross sections to be determined across a larger missing momentum range than the central value kinematic settings would suggest.

The electron spectrometer was fixed in angle and central momentum while the proton spectrometer's angles and central momenta were changed. The electron arm settings are in table I. The proton arm settings are in table II.

B. Cryogenic target

The cryogenic target was ^4He contained in an aluminum can of length 20 cm. The nominal temperature of the gas was 20° K at 199 psia. ^4He enters and exits at

* Corresponding author: kaniol@calstatela.edu

incident beam energy	4.4506 GeV
electron spectrometer angle	20.3°
electron spectrometer momentum	3.602 GeV/c
Q^2	2.0 $(GeV/c)^2$
Bjorken x_b	1.24

TABLE I. Electron spectrometer kinematic settings for E08009.

Central P_{miss}	θ_p	Central momentum
GeV/c	degrees	GeV/c
0.153	47.0	1.500
0.353	38.5	1.449
0.466	33.5	1.383
0.632	29.0	1.308

TABLE II. Proton spectrometer settings

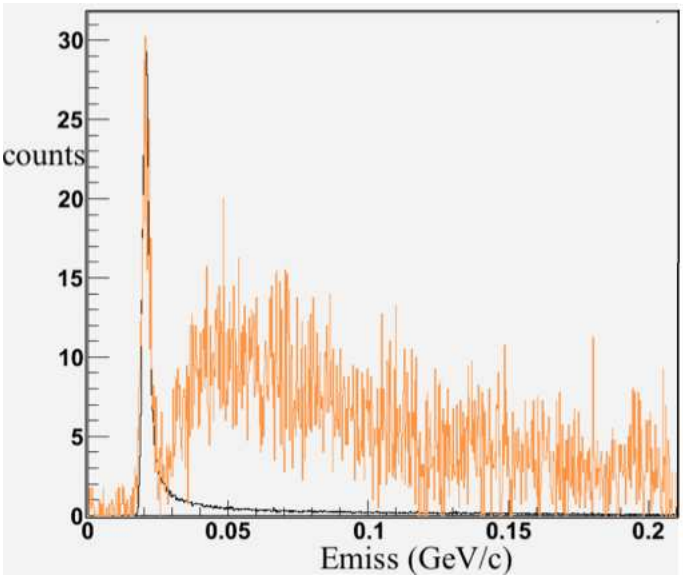

FIG. 1. Missing energy spectrum for the $p_m = 0.353\ GeV/c$ kinematic setting, $\theta_p = 38.5°$. Data in color, Simulation in black.

the upstream end of the target. There is no outlet for the fluid at the downstream end of the can. A determination of target density along the beam path was possible by comparing the normalized yield of scattered electrons at $47\mu A$ and $60\mu A$ beam currents to the yield at $4\mu A$. Since the electron spectrometer was held at a fixed momentum and angle the electron spectrometer served as a density monitor. For this target at a beam current of $4\mu A$ a computational fluid dynamics(CFD) calculation [5] predicts an average density drop of 2.3% from strictly thermodynamic parameters. A comparison of the measured yield at $4\mu A$ to the CFD calculation gives an uncertainty in the target density dependence along the beam of 1.1%. More detail for the treatment of the target density used in the data analysis is available in [3] and [4].

III. DATA ANALYSIS

Data analysis is guided by the Monte Carlo simulation(GEANT 3.2) of the transport of the incident electron, scattered electron and proton through the target cell into the spectrometer apertures assuming a p + triton final hadronic state. The identification of the p + triton final state is possible by calculating the missing energy in the scattered electron + p state. The missing energy is the kinetic energy carried off by the undetected system X in $^4He(e,e'p)X$ reaction. A peak in the missing energy corresponding to the triton ground state mass identifies the $^4He(e,e'p)^3H$ reaction, where m_X = triton mass..

A. Radiative effects

Radiative effects, obtained from the GEANT simulation including internal and external bremsstrahlung, produce a broadening and a characteristic tail on the missing energy spectrum. In practice the long target introduces additional broadening beyond the intrinsic point source resolution of the spectrometers. The additional broadening is included in the simulation by a Gaussian broadening of the momenta at the apertures predicted from the simulation. This additional broadening typically is a factor of three to four bigger than the resolution for the point source resolution. The amount of Gaussian smearing needed is determined by the best fit of a strong missing energy data peak such as at the lowest missing momentum. An example of the fit is seen in figure 1.

Radiative corrections to the cross section are determined from the simulation by comparing the number of events in a 5 MeV window centered on the triton peak to the total number of events in the simulation.

B. Missing momentum acceptance efficiency

The wide momentum acceptance of the spectrometers allows for a broad missing momentum acceptance. In the simulation a vertex point in the gas target is chosen and the hit points within the apertures of the spectrometers for the outgoing electron and proton are randomly selected. Each point within the spectrometers' apertures has an equal probability of being selected. This allows for the vertex angles of the electron and proton to be determined. An energy for the outgoing electron is chosen within the momentum acceptance of the electron spectrometer. From the electron's scattering angle the outgoing electron's energy is adjusted for internal bremsstrahlung. Three body kinematics for the

parameters	value for electron and proton spectrometers
horizontal angle	±0.04 radians
vertical angle	±0.03 radians
vertex position	±8 cm
deviation from central momentum	±0.06 %

TABLE III. Cuts applied to the data for cross section determinations.

$^4He(e,e'p)^3H$ reaction allows for the proton's vertex momentum to be determined. The electron and proton are followed from the vertex to the final hit points in the spectrometers' apertures. Thus complete information about the location and momenta at the vertex and the spectrometers' apertures is known.

The three body kinematical and geometrical limitations for particles arriving at the hit points within the apertures are correctly calculated by GEANT and thus allows the missing momentum, $\vec{p_m} = \vec{p_1} - \vec{p_2} - \vec{p_p}$ to be calculated. In the analysis we bin $|\vec{p_m}|$ into 50 MeV/c bins. We define the missing momentum acceptance factor, $f(p_m)$, for a bin of missing momentum centered around p_m as

$$f(p_m) = \frac{n(p_m)}{\sum n(p_m)}. \quad (1)$$

where $n(p_m)$ is the number of triton events in the missing momentum bin centered on p_m and $\sum n(p_m)$ is the total number of triton events over all missing momenta for the particular proton kinematic setting. The same Gaussian broadening used for the simulation fit in figure 1 is used to generate the values of p_m needed to calculate $f(p_m)$.

Cuts on the data are given in table III.
Experimental cross sections are given in table IV.

IV. RESULTS

A. Comparison of data to theoretical predictions

Experimental differential cross sections are compared to relativistic distorted wave impulse approximation calculations of the Madrid theory group [6], [7], [8], [9]. The ^4He ground state is described with realistic nucleon-nucleon interactions using the adiabatic hyper-spherical expansion method [8]. Nucleons are described by the Dirac equation with scalar and vector(S-V) potentials. The outgoing proton wave function is obtained by solving the Dirac equation with a S-V optical potential fitted to proton scattering on ^3H.

Vertex values of the incident electron's momentum at various positions within the target and the momenta of the scattered electron and ejected proton were provided to the Madrid theory group for calculation of the cross section at each event vertex in the GEANT simulation. The GEANT simulation also contains the detected electron and proton momenta at the spectrometers' apertures. In this way the vertex cross section can be associated with the missing momentum at the apertures. The GEANT simulation includes external and internal bremsstrahlung. Theoretical cross sections integrated over the experimental acceptances for the full Madrid treatment and using the effective momentum approximation(EMA) treatment are in tables V and VI. Plots of the data for the two theoretical treatments are shown in figures 2 and 3.

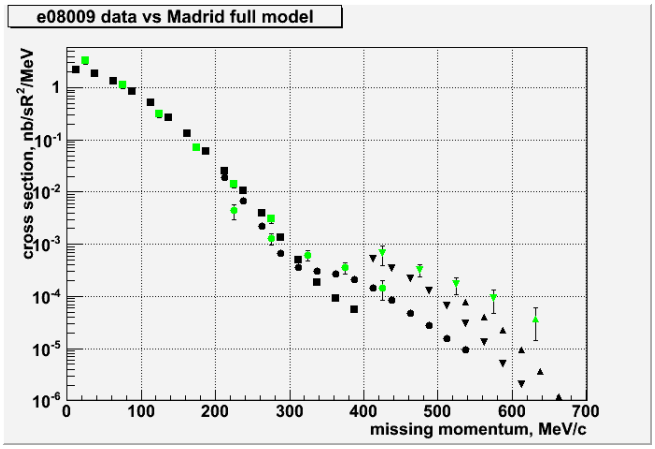

FIG. 2. E08009 Data in green compared to full Madrid theoretical calculations in black. Squares are for the 153 MeV/c setting, circles are for 353 MeV/c setting, inverted triangles are for the 466 MeV/c setting and triangles are for the 632 MeV/c setting.

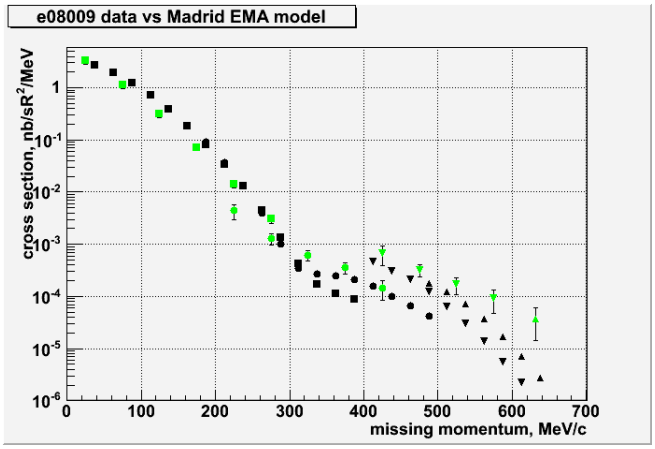

FIG. 3. E08009 Data in green compared to EMA Madrid theoretical calculations in black. Squares are for the 153 MeV/c setting, circles are for 353 MeV/c setting, inverted triangles are for the 466 MeV/c setting and triangles are for the 632 MeV/c setting.

P_{miss} (MeV/c)	153 $\theta_p = 47°$	353 $\theta_p = 38.5°$	466 $\theta_p = 33.5°$	632 $\theta_p = 29°$
25	(3.38 ± 0.52)			
75	(1.13 ± 0.17)			
125	$(3.13 \pm 0.48) \times 10^{-1}$			
175	$(7.18 \pm 1.1) \times 10^{-2}$			
225	$(1.44 \pm 0.22) \times 10^{-2}$	$(4.40 \pm 0.14) \times 10^{-3}$		
275	$(3.06 \pm 0.57) \times 10^{-3}$	$(1.27 \pm 0.03) \times 10^{-3}$		
325		$(6.11 \pm 0.14) \times 10^{-4}$		
375		$(3.57 \pm 0.88) \times 10^{-4}$		
425		$(1.44 \pm 0.59) \times 10^{-4}$	$(6.59 \pm 2.7) \times 10^{-4}$	
475			$(3.22 \pm 0.89) \times 10^{-4}$	
525			$(1.68 \pm 0.45) \times 10^{-4}$	
575			$(0.91 \pm 0.43) \times 10^{-4}$	
632				$(3.7 \pm 2.3) \times 10^{-5}$

TABLE IV. Experimental differential cross sections, $\frac{d\sigma^5}{d\Omega_p d\Omega_e dE_e}$, for $^4He(e,e'p)^3H$ from E08009, for different kinematical settings given by the proton spectrometer central angle. Units are $nb/sr^2/MeV$.

The data and calculations show the same missing momenta dependence on the measured or calculated cross section as a function of kinematic setting. Even though the same magnitude of p_m is reached for different proton angles the cross section does not simply factor into a function of p_m. Good fits between the Madrid calculation and the data go out to about 420 MeV/c in missing momentum. Data and theory exhibit a break in the slope of the cross section between 300 and 400 MeV/c. In a recent calculation [1] of the proton momentum distribution in ^4He a break in the momentum slope is predicted in this missing momentum range. The origin of this break in the slope appears to be due to the triton+proton cluster distribution [1] exhibiting a deep minimum in the proton momentum distribution at about 453 MeV/c.

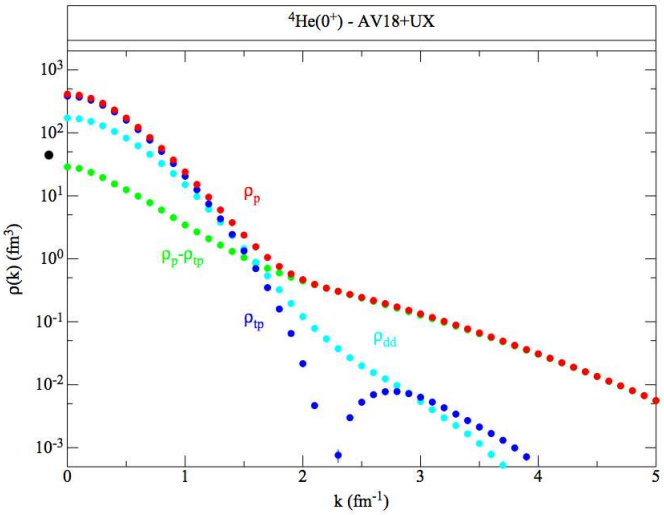

FIG. 4. Proton momentum density taken from [1] website showing contributions to the proton momentum density from the tp and dd cluster.

V. DISCUSSION

The data that are actually measured in this experiment are the three momenta of the outgoing proton and electron. The full experiment is $^4He(e,e'p)X$. Using the known momentum of the initial state we deduce the missing momentum of the residual hadronic state X. The theoretical analysis of the data here is limited to a specific exit channel, $X = {}^3H$. However, considering the theoretical cluster contributions to the proton momenta [1] in ^4He, shown in figure 4, the contribution of the pt cluster to the proton momentum distribution is expected to be negligible above about $p_m = 250$ MeV/c.

From figure 4 the high proton momentum is attributed to the repulsive nucleon-nucleon core [1]. The measurements of [2] are consistent with the NN short range force becoming repulsive. However, it is counter intuitive and in disagreement with theoretical expectations [1] that tritons should be ejected from ^4He along with protons emerging from short range encounters.

The fact that we observe events in the triton region out to 632 MeV/c involves processes beyond the impulse approximation. Final state interactions of the outgoing proton may take a proton knocked out of a pt cluster initially at a low value of p_p to appear as if its momentum at the vertex was p_m. This is accounted for to some extent by the optical potential treatment of the final pt unbound state. We see good agreement between the theory and

P_{miss} (MeV/c)	153 $\theta_p = 47°$	353 $\theta_p = 38.5°$	466 $\theta_p = 33.5°$	632 $\theta_p = 29°$
12.5	2.20585	0	0	0
37.5	1.82871	0	0	0
62.5	1.31389	0	0	0
87.5	0.851553	0	0	0
112.5	0.506994	0	0	0
137.5	0.26989	0	0	0
162.5	0.131086	0	0	0
187.5	0.0598725	0	0	0
212.5	0.0258303	0.0191822	0	0
237.5	0.010439	0.0067236	0	0
262.5	0.00395091	0.00220872	0	0
287.5	0.00137024	0.000668576	0	0
312.5	0.000490056	0.000357781	0	0
337.5	0.000185816	0.000309488	0	0
362.5	9.30929e-05	0.00026867	0	0
387.5	5.63916e-05	0.000207743	0	0
412.5	0	0.000141879	0.000528339	0
437.5	0	8.3657e-05	0.000340153	0
462.5	0	4.80785e-05	0.000222462	0
487.5	0	2.73925e-05	0.000126155	0.0002206
512.5	0	1.54183e-05	6.54197e-05	0.0001491
537.5	0	9.47828e-06	2.97952e-05	8.585e-05
562.5	0	0	1.28925e-05	4.4e-05
587.5	0	0	5.07677e-06	1.977e-05
612.5	0	0	2.00828e-06	7.741e-06
637.5	0	0	8.3571e-07	2.834e-06

TABLE V. Madrid full theoretical cross sections integrated over the experimental acceptances for $^4He(e,e'p)^3H$ for E08009, for different kinematical settings given by the proton spectrometer central angle. Units are $nb/sr^2/MeV$.

P_{miss} (MeV/c)	153 $\theta_p = 47°$	353 $\theta_p = 38.5°$	466 $\theta_p = 33.5°$	632 $\theta_p = 29°$
12.5	0	0	0	0
37.5	2.681	0	0	0
62.5	1.916	0	0	0
87.5	1.235	0	0	0
112.5	0.729652	0	0	0
137.5	0.383898	0	0	0
162.5	0.183412	0	0	0
187.5	0.0815901	0.0903122	0	0
212.5	0.0338215	0.0362774	0	0
237.5	0.0128213	0.0129471	0	0
262.5	0.00443289	0.0039332	0	0
287.5	0.00136237	0.000998639	0	0
312.5	0.000431068	0.000342315	0	0
337.5	0.000170451	0.000264277	0	0
362.5	0.000112972	0.00024869	0	0
387.5	8.81671e-05	0.00020829	0	0
412.5	0	0.000154708	0.000455009	0
437.5	0	9.85333e-05	0.000308199	0
462.5	0	6.48162e-05	0.000206383	0
487.5	0	4.26083e-05	0.000120555	0.0001778
512.5	0	0	6.4348e-05	0.0001215
537.5	0	0	3.03616e-05	7.084e-05
562.5	0	0	1.35952e-05	3.702e-05
587.5	0	0	5.52707e-06	1.717e-05
612.5	0	0	2.25103e-06	7.01e-06
637.5	0	0	9.48271e-07	2.695e-06

TABLE VI. Madrid EMA theoretical cross sections integrated over the experimental acceptances for $^4He(e,e'p)^3H$ for E08009, for different kinematical settings given by the proton spectrometer central angle. Units are $nb/sr^2/MeV$.

data in figure 2 up to about $p_m = 420\ MeV/c$. Beyond about 450 MeV/c in P_{miss} substantially more triton region events are measured than our theory predicts. The ratio of experimental cross section to theoretical prediction is shown in figure 5.

In this case tritons emitted at high p_m may be a signature of other reactions allowing the three nucleon cluster to emerge as a bound or quasi bound state. Since the kinematics for the electron were chosen for $x_b = 1.24$, protons in more intimate interactions with neighbors than quasi-elastic conditions($x_b \approx 1$) may favor other reactions leading to three nucleon clusters exiting in the missing energy region associated with the triton. Portions of the missing energy spectrum in the triton energy range are shown in figures 6, 7, 8 and 9.

An interesting question is the impact of three-nucleon forces, V_{ijk}, at high p_m. V_{ijk} are known to increase the binding energy of nuclei [10] so they would be natural actors in the formation of bound tritons or closely

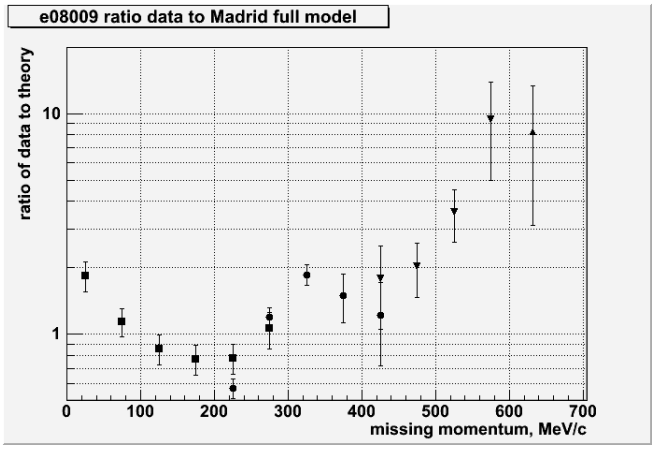

FIG. 5. Ratio of the experimental cross section to the theoretical Madrid cross section versus missing momentum. Squares are for the 153 MeV/c setting, circles are for 353 MeV/c setting, inverted triangles are for the 466 MeV/c setting and triangles are for the 632 MeV/c setting.

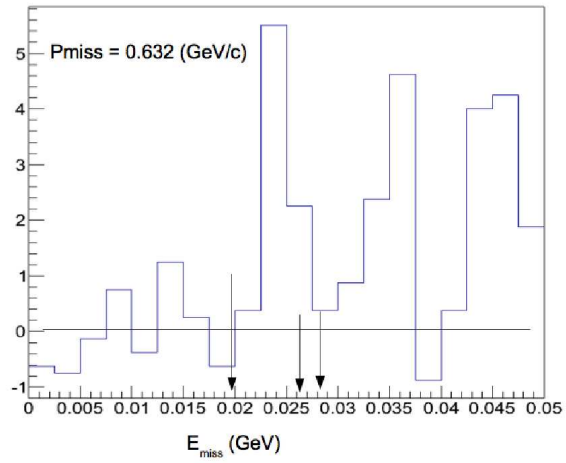

FIG. 6. Missing energy region up to 50 MeV of excitation in $^4He(e,e'p)X$ for $P_{miss} = 632 MeV/c$. The three arrows point to the expected locations of hadronic states X=(t), X=(n,d) and X=(p,n,n).

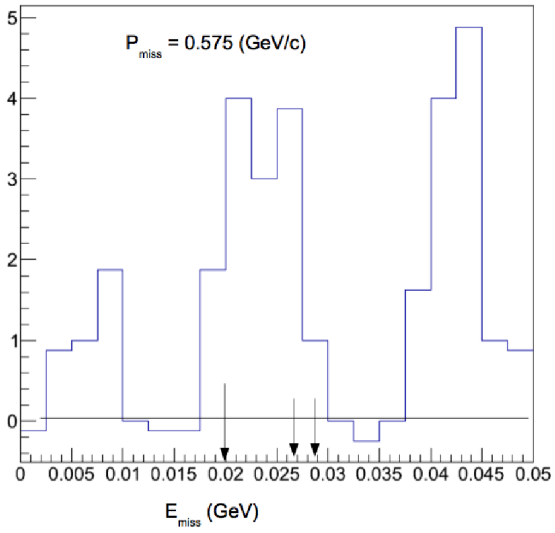

FIG. 7. Missing energy region up to 50 MeV of excitation in $^4He(e,e'p)X$ for $P_{miss} = 575 MeV/c$. The three arrows point to the expected locations of hadronic states X=(t), X=(n,d) and X=(p,n,n).

bound three nucleon groups among the outgoing hadronic channels, X, at high missing momentum. The principal sources of data to help refine models of possible three-nucleon interactions are binding energies of ground and excited states of $A < 8$ nuclei and point proton charge distributions [10]. However, these data are not extensive enough unambiguosly to select a particular set of parameters or models for V_{ijk} and other observables are needed as discussed in [10] [11].

More extensive and detailed data in the three nucleon triton mass region and the existence of microscopic calculations for these nuclei opens the possibility of exploiting the $A(e,e'pt)X$ reactions as additional observables for developing models of three-nucleon interactions.

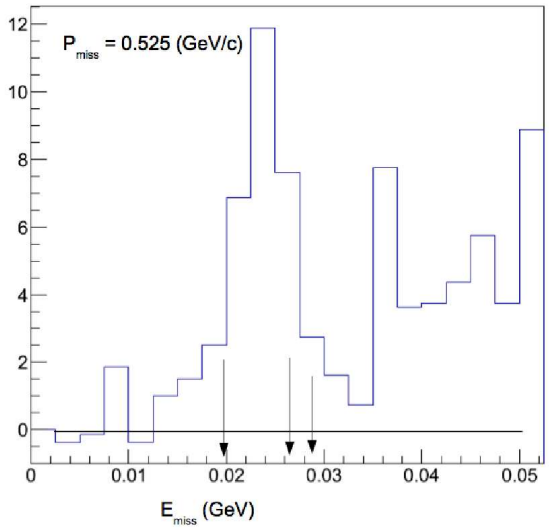

FIG. 8. Missing energy region up to 50 MeV of excitation in $^4He(e,e'p)X$ for$P_{miss} = 525 MeV/c$. The three arrows point to the expected locations of hadronic states X=(t), X=(n,d) and X=(p,n,n).

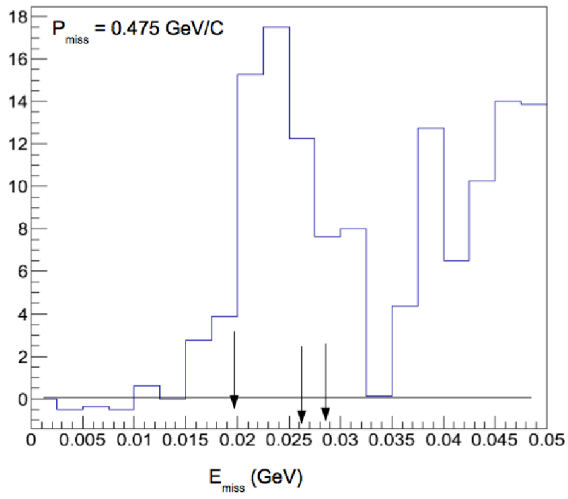

FIG. 9. Missing energy region up to 50 MeV of excitation in $^4He(e,e'p)X$ for$P_{miss} = 475 MeV/c$. The three arrows point to the expected locations of hadronic states X=(t), X=(n,d) and X=(p,n,n).

[1] R. B. Wiringa and *et al.*, Phys. Rev. C, **89**, 024305 (2014).
[2] I. Korover and *et al.*, Phys. Rev. Lett., **113**, 022501 (2014).
[3] Sophia Iqbal, California State University, Los Angeles (2013), https://misportal.jlab.org/ul/publications/downloadFile.cfm?pub_id=13189,unpublished.
[4] K. A. Aniol, N. Y. See and S. Iqbal (2013), https://userweb.jlab.org/ aniol/e08009/iscan_corrections/SRCtgt.pdf,unpublished.
[5] Siviu Covrig, Computational Fluid Dynamics, private communication (2012).
[6] J. Udías and *et al.*, (2013), arXiv:0109077v1 [nucl=th].
[7] S. P. Malace and *et al.*, Phys. Rev. Lett., **106**, 052501 (2011).
[8] R.Álvarez-Rodríguez and *et al.*, (2010), arXiv:10123.3049v1 [nucl-th].
[9] J. M. Udias and J. R. Vignote, Phys. ReV. C, **62**, 034302 (2000).
[10] S. Pieper and *et al.*, Phys. Rev. C, **64**, 014001 (2001).
[11] D. Lonardoni and *et al.*, (2017), arXiv:1705.04337v1 [nucl-th].